Available online at www.sciencedirect.com
ScienceDirect
Trans. Nonferrous Met. Soc. China 29(2019) 1242−1251
Transactions of Nonferrous Metals Society of China
www.tnmsc.cn

Precipitation response and hardening behaviors of Fe-modified Ti5553 alloy

Wen-guang ZHU[1], Pei LI[1], Xun SUN[2], Wei CHEN[1], Hua-lei ZHANG[2], Qiao-yan SUN[1], Bin LIU[3], Lin XIAO[1], Jun SUN[1]

1. State Key Laboratory for Mechanical Behavior of Materials, Xi'an Jiaotong University, Xi'an 710049, China;
2. Frontier Institute of Science and Technology, Xi'an Jiaotong University, Xi'an 710049, China;
3. State Key Laboratory of Powder Metallurgy, Central South University, Changsha 410083, China

Received 7 September 2018; accepted 4 March 2019

Abstract: Ti5553−xFe (x=0.4, 1.2, 2.0, wt.%) alloys have been designed and fabricated through BE (blended element) sintering to investigate the effect of Fe-addition on athermal ω-phase transformation, α-phase evolution and age hardening behavior. The results show that the formation of athermal ω-phase is fully suppressed in water-quenched specimens when Fe-addition is up to 2 wt.%. The relevant timescales of α formation during initial stages of aging indicate that incubation time increases with Fe-addition. Further aging results in continuous nucleation and growth of α-phase but finer intragranular α lamellae exhibit in Ti5553−2Fe alloy. In addition, the width and extent of grain boundary α-film increase slightly with incremental Fe-addition, especially in furnace cooling condition. Result of Vickers hardness manifests that Fe-addition leads to a strong hardening effect in both solution and aging treatment. The solid solution strengthening is quantitatively estimated by *ab initio* calculation based on the Labusch−Nabarro model. The evolution of α-precipitate is rationalized by Gibbs free energy. The prominent hardening effect of Ti5553−2Fe alloy is attributed to both large lattice misfit of β-matrix and fine α-precipitate distribution.

Key words: Fe-modified Ti5553 alloy; α-phase evolution; hardening behavior; Pandat calculation

1 Introduction

β-Ti alloys have been becoming increasingly attractive for high strength structural components in aerospace applications since the first commercial β titanium alloy Ti-13-11-3 was developed in 1952 and applied successfully in SR-71 [1−3]. This type of alloy possesses an excellent combination of strength−toughness−fatigue resistance and affordable thermo-mechanical processing [4−6]. Particularly, for near β titanium alloys, they incorporate both the advantages of α/β two phase alloys and β alloys by means of appropriately thermo-mechanical processing [2,7]. Hence, more attention has been attracted on the study of near β-Ti alloys in research community [8].

Similar to dual phase steel in which the ferrite matrix is strengthened by martensite during cooling from FCC austenitic phase, near β-Ti alloys are mainly hardened by the precipitation of fine α-particles from the supersaturated β-matrix [9]. In addition, β-matrix can also be strengthened by the solutes of β-stabilizers such as Mo, V, Cr and Fe, which in turn effectively changes the precipitation behavior of α phase. Recently, owing to the strong strengthening effect and relative low cost of Fe element, several attempts have been made to get insight into its role in microstructure evolution and deformation behavior [10−14]. Ultra-high ultimate tensile strength of ~1690 MPa can be achieved in a low-cost β-Ti alloy Ti−1Al−8V−5Fe. The high strength originates from hierarchical microstructure consisting of homogenous distribution of micron-scale and nanoscale α-phase precipitates induced by Fe-addition [11]. CHEN and HWANG [15], BOLZONI et al [12] and HSU et al [16] investigated the effect of Fe in Ti−Fe binary system where α-lamellae became finer with increasing Fe content. In addition, the effect on deformation mode of high strength β-Ti alloy is also investigated. MIN

Foundation item: Projects (51671158, 51871176, 51621063) supported by the National Natural Science Foundation of China; Project (2014CB644003) supported by the National Basic Research Program of China; Project (PB2018008) supported by the 111 Project 2.0, China; Project (2018JM5098) supported by the Natural Science Basic Research Plan in Shaanxi Province of China
Corresponding authors: Qiao-yan SUN, Tel: +86-13002912355, E-mail: qysun@xjtu.edu.cn;
Wei CHEN, Tel: +86-13389213172, E-mail: weichen813@xjtu.edu.cn
DOI: 10.1016/S1003-6326(19)65031-4

et al [17−19] observed the suppression of athermal ω-phase and the deformation mode changing from <113> twinning to only slip with increasing Fe content in Ti−15Mo system. However, the aforementioned investigations mainly involve the effect of Fe on α-phase refinement and deformation behavior. The insight of strengthening mechanism and the evolution of α-phase which referred to thermodynamics and diffusion is relatively scarce.

Ti−5Al−5Mo−5V−3Cr (Ti5553) is a novel β-Ti alloy which has been successfully applied in landing gear forgings due to less sensitive to thermo-mechanical temperature and improved hardenability in comparison to Ti-1023 alloy [20]. Transformation mechanism and Correlation among processing, microstructure and mechanical property have been well documented [21−24]. Recently, the micro-alloying of Ti5553 alloy is becoming a new attractive field. QIN et al [25] investigated the effect of Si addition to Ti5553 alloy. The results showed a slightly increase in ultimate tensile strength but a decrease in ductility owing to the refined α-phase precipitation. In other investigations, Ti5553 alloy was modified by the addition of C and B, which led to a finer microstructure and an increase in mechanical strength. OPINI et al [26] and CAMPO et al [27] investigated the effect of Nb on α-phase morphology and mechanical properties. The results indicated that Nb-modified alloy exhibited improved mechanical strength but lower ductility. However, as one of the strongest β-stabilizers mentioned above, there is no publication regarding the effect of Fe-addition in Ti5553 alloy.

In this study, the effect of Fe-additions on precipitation response and strengthening behavior in Ti5553 alloy is investigated. The microstructure evolution and corresponding hardening behavior with incremental Fe-additions are discussed. The results shed light on the capability of Fe-addition in enhancing mechanical properties of Ti5553 alloy and provide a guideline for composition design of high strength β-Ti alloys.

2 Experimental

The Ti5553−xFe alloys with x=0, 0.4, 1.2, 2.0 (wt.%) were designed and sintered using blended element (BE) method. The powders in the form of hydride−dehydride (HDH) Ti powders, 60V−40Ti master alloy powders and Al, Cr, Mo powders were blended with Fe powders in SPEX 8000M mixer for 3 h with shielding argon gas. The general parameters of these powders are listed in Table 1. Cold isostatic pressing was performed under a pressure of 200 MPa and the compacts were then sintered at 1250 °C for 3 h in high vacuum of ~1.0×10^{-3} Pa. Subsequently, hot forging was conducted at a temperature around 1050 °C with approximately 60% deformation. Finally, the forged billets were solid solution treated at 1000 °C for 1 h and water quenched followed by aging at 600 °C for various time from 5 min to 24 h.

Table 1 Preparation method of powders for sintering

Powder	Particle size/μm	O content/ wt.%	Preparation method
Ti	62.72	0.14	Hydride−dehydride
Mo	4.64	0.28	Reduction oxide
Cr	32.18	0.39	Reduction oxide
Al−V	50.82	0.30	Disintegration of master alloy
Fe	38.47	0.13	Carbonyl decomposition

In order to observe the microstructural evolution, specimens were mechanically ground on a metallographic sandpaper, electrochemical polished and etched in a Kroll's reagent. Microstructural characterization was performed on Nikon ECLIPSE MA200 optical microscopy (OM), Hitachi SU6600 scanning electron microscopy (SEM) and JEOL JEM−2100F transmission electron microscopy (TEM), respectively. X-ray diffraction (XRD) analysis for phase transformation was conducted by applying a Bruker D8 Advance diffractometer with Cu K_α radiation. Vickers hardness of polished specimens was measured under a load of 5 kg and at least ten indentations for each specimen were measured for average.

3 Results

3.1 $\beta\rightarrow\alpha$ phase transformation during furnace cooling

Figure 1 shows the characteristic microstructure of Ti5553 alloy after furnace cooling from 1250 °C. Typical Widmannstatten structure composed of continuous grain boundary α (α_{GB}) and distinct α side plates is formed regardless of Fe-content. However, the width and extent of α_{GB} and α side plates increase with incremental Fe-addition (Figs. 1(a, c, e)) while the size of intragranular α becomes finer (Figs. 1(b, d, f)). This feature indicates that Fe-addition promotes the nucleation and growth of α phase along grain boundaries but suppresses the growth of intragranular α-phase. The results were also observed in Nb-modified Ti5553 alloy [26,27]. In addition, it should be noted that the precipitation free zone (PFZ) appeared near the α_{GB} and side plates in Fig. 1(c), which is probably due to the enhanced adjacent β phase stability as a result of the high diffusion rate of Fe-element.

3.2 Precipitation behavior of as-solid solution-treated specimens

Figure 2 shows microstructural characteristics and XRD patterns of the as-solution-treated specimens. The microstructure is composed of single β phase irrespective of Fe-addition, as shown in Fig. 2(a). XRD patterns detected neither the intensive $\{10\bar{1}1\}_\omega$ reflection which is adjacent to $\{110\}_\beta$ peak nor the distinctive $\{11\bar{2}2\}_\omega$ peak around 79° (Fig. 2(c)). The lacking of ω reflection is due to low-precision of traditional XRD which cannot detect the faint diffraction peak of the nano-scale ω-phase with less amount. Nevertheless, using TEM microscopy, athermal ω-phase is observed inside β-matrix of Fe-free Ti5553 specimen, as shown in

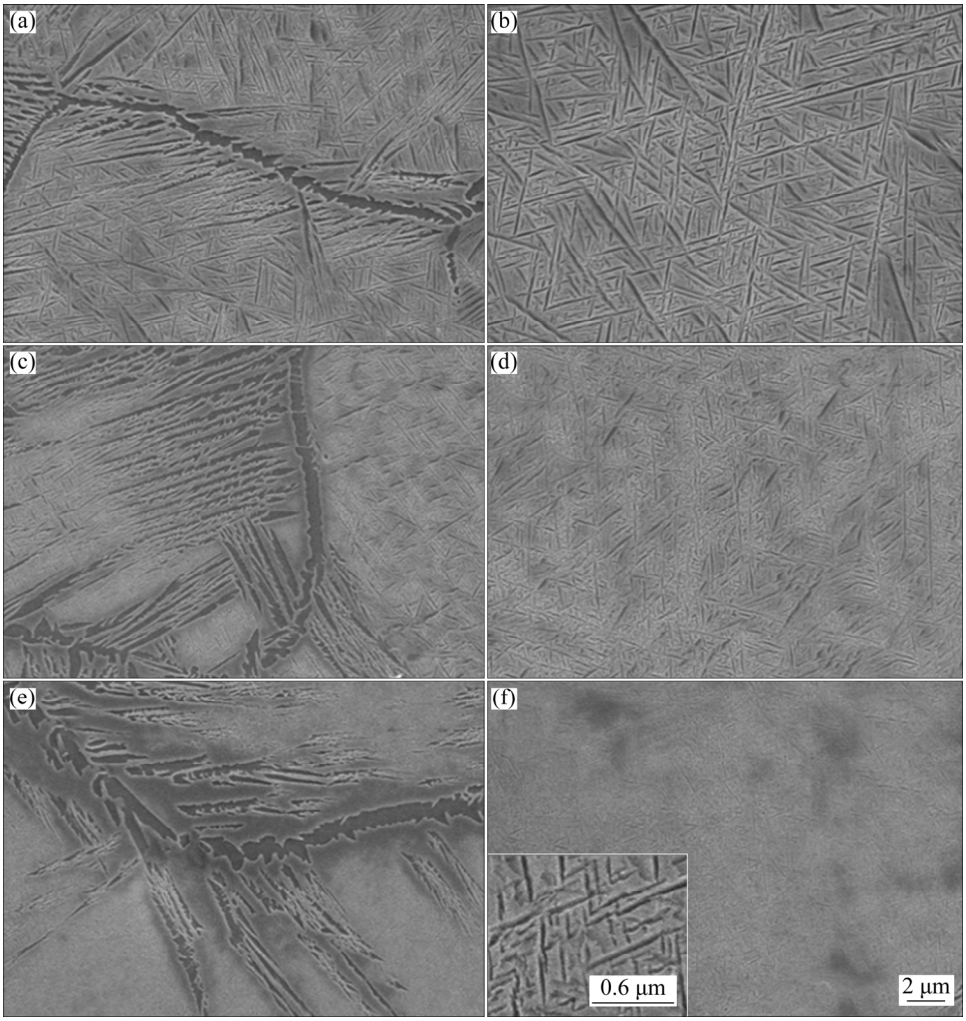

Fig. 1 Microstructures of Ti5553 alloy with different Fe additions after furnace cooling from 1250 °C: (a, b) Fe-free Ti5553; (c, d) Ti5553-0.4Fe; (e, f) Ti5553-2Fe ((a, c, e) represent morphology of grain boundary α and adjacent side plates; (b, d, f) represent intragranular α lamella)

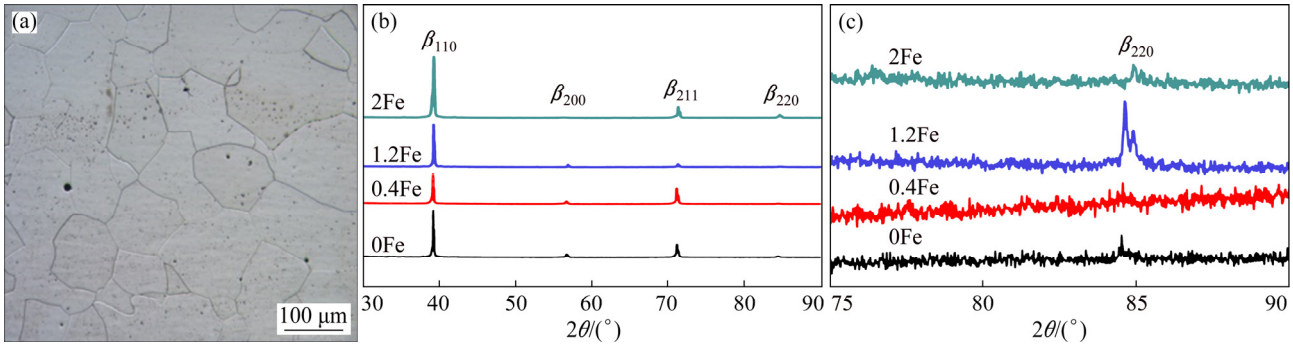

Fig. 2 Characterization of Ti5553−xFe alloy after solid solution treatment at 1000 °C for 1 h: (a) Optical microstructure of β grains; (b) XRD pattern of samples; (c) Close-up XRD pattern without presence of $\{11\bar{2}2\}_\omega$ diffraction peak around 79°

Fig. 3(a). The faint reciprocal lattice streaking (RLS) is presented in the selected area electron diffraction pattern (SAED). The reflections at 1/3 and 2/3$\{112\}_\beta$ positions of the $[011]_\beta$ zone axes in shape of the faint diffused streaked "x" correspond to two specific ω variants. Furthermore, a dark-field TEM image obtained from the RLS is shown in Fig. 3(b). It is observed that nano-scale ω-precipitates homogeneously distribute throughout β-matrix. When modifying Ti5553 alloy with Fe-addition, the formation of athermal ω-phase is gradually suppressed. Figures 3(c) and (d) show that neither the faint RLS nor the 1/3 and 2/3$\{112\}_\beta$ position reflections could be observed along the $[011]_\beta$ and $[\bar{1}13]_\beta$ zone axis in Ti5553−2Fe specimens. This indicates that 2 wt.% addition of Fe significantly enhances β phase stability, resulting in the full suppression of athermal ω-phase.

3.3 α-precipitation behavior during aging

SEM images of Ti5553−xFe specimens aged at 600 °C for 5 min are shown in Fig. 4. A large amount of α phases, nearly 1 μm in length, generally exhibit in the Fe-free Ti5553 specimen (Fig. 4(a)). However, there is a significant decrease in density and size in Ti5553−1.2Fe specimen. Furthermore, no α-precipitate exhibits when Fe content is increased to 2 wt.% for 5 min aging (Fig. 4(d)). This feature is consistent with the result of XRD pattern where only β-diffraction peaks appear (Fig. 4(e)), which indicates that Fe-addition could effectively postpone the aging response of α-precipitates. Moreover, as shown in both Fe-free Ti5553 (Fig. 4(a)) and Ti5553−1.2Fe specimens (Fig. 4(b)), amounts of triangular-shaped clusters of α phase are preferentially precipitated. The clusters represent three specific variants owing to the self-accommodation of elastic strain during phase transformation [23]. The formation process is proposed to involve $[11\bar{2}0]_\alpha/60°$ variants by which three variants grow with three $\{0001\}_\alpha//\{011\}_\beta$ lying at 60° to each other and share a common $\langle 11\bar{2}0\rangle_\alpha//\langle 111\rangle_\beta$ direction [23,28]. Figures 4(a−c) show a coexistence of micron-scaled and nano-scaled α-precipitates. It is reasonable to assume that after the first batch of $\langle 11\bar{2}0\rangle_\alpha/60°$ variants precipitated within β-matrix, the adjacent β-matrix becomes stable due to the injection of β-stabilizers, in turn, resulting in a finer α-precipitates by sympathetic nucleation.

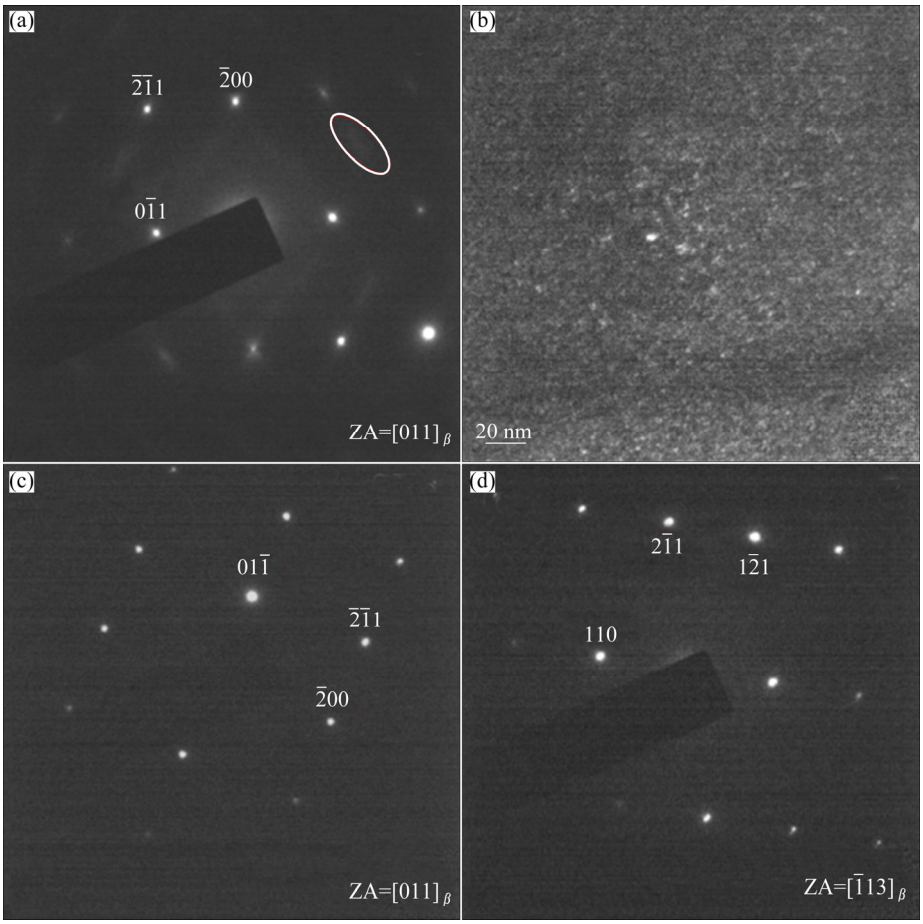

Fig. 3 SAED patterns and DF TEM image of as-solution-treated Ti5553−xFe specimens: (a) SAED pattern along $[110]_\beta$ zone axis for Ti5553; (b) Corresponding DF TEM image of athermal ω-precipitates for Ti5553; (c, d) SAED patterns along $[110]_\beta$ and $[\bar{1}13]_\beta$ zone axis for Ti5553−2Fe specimens

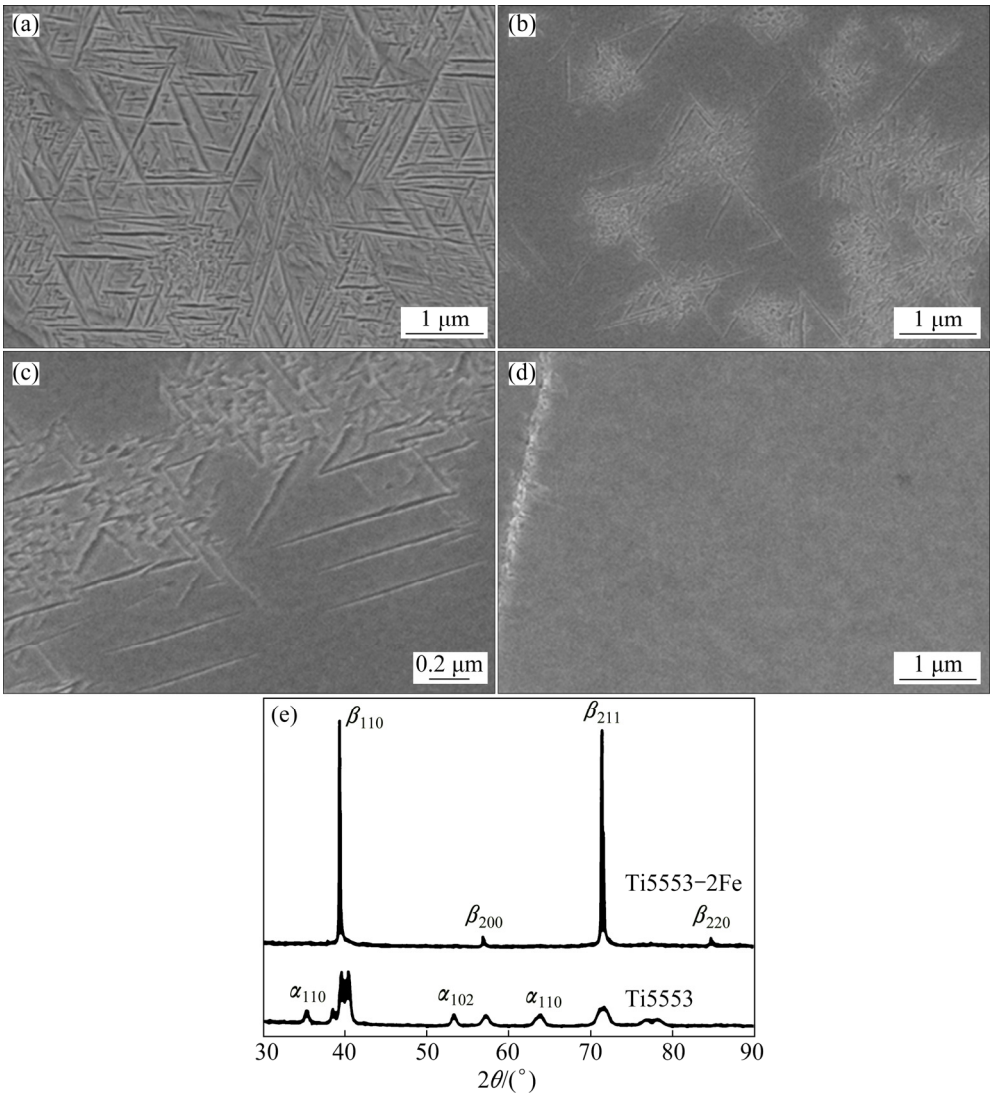

Fig. 4 SEM images and XRD patterns of Ti5553−*x*Fe specimens aged at 600 °C for 5 min: (a) Fe-free Ti5553 alloy; (b) Ti5553−1.2Fe; (c) Local magnification of (b); (d) Ti5553−2Fe; (e) XRD patterns of Fe-free Ti5553 and Ti5553−2Fe specimens

Figure 5 shows SEM morphologies of Ti5553−*x*Fe specimens aged at 600 °C for 1 h. As expected, α-precipitates continuously grow and coarsen with aging time. The size of α precipitates, especially in length, is slightly finer in Ti-5553-2Fe than in Fe-free specimen. This phenomenon is consistent with the refinement effect as reported in Ti−Fe binary system and Ti−Nb−Fe system [13,15]. The fast diffusion rate of Fe in β-Ti alters the kinetics of α precipitates. The rejection of Fe from α-phase leads to an enrichment in the adjacent β matrix, which suppresses the growth of α-lamella and results in finer α-precipitates during aging. Figures 5(c) and (d) show the morphology of grain boundary α (α_{GB}) of Ti5553 and Ti5553−2Fe specimens, respectively. The film of α_{GB} is more continuous in Ti5553−2Fe specimen, indicating that Fe promotes the tendency of α-precipitates nucleation and growth along grain boundary.

Figures 6(a−c) show the microstructures of Ti5553−*x*Fe specimens after 6 h aging. By comparing specimens with different Fe-additions, the length of α-precipitates reduces with the increase of Fe content, similar to the case in Fig. 4 and Fig. 5. The statistical analysis by Image-Pro Plus shows that volume fraction of α phase in Ti5553 and Ti5553−2Fe after (600 °C, 6 h) aging is 20% and 21%, respectively. The density of α lamella is approximately unchanged (23.01 μm^{-2} in Ti5553 and 22.56 μm^{-2} in Ti5553−2Fe). However, the density of lamella α with length over 1 μm is 1.32 μm^{-2} in Fe-free alloy and 0.31 μm^{-2} in Ti5553−2Fe alloy, respectively. This means that Fe-addition decelerates α-growth while has little influence on volume fraction and density of α in 6 h aging. This assertion is validated in samples with longer aging time of 24 h, as shown in Figs. 6(d−f), where it is little change of volume fraction and density except slight coarsening of α-lamella.

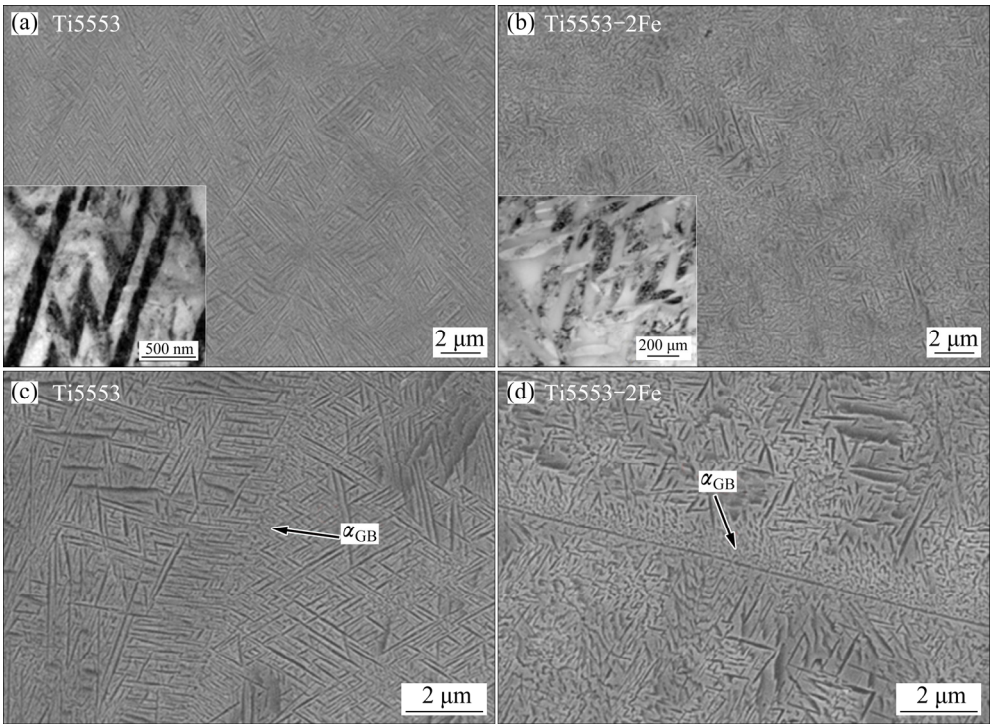

Fig. 5 α-phase morphologies of Ti5553−xFe aged at 600 °C for 1 h: (a, b) Intragranular α lamella with inserted TEM images for Fe-free Ti5553 and Ti5553−2Fe specimens, respectively; (c, d) Grain boundary α along β grain for Fe-free Ti5553 and Ti5553−2Fe specimens, respectively

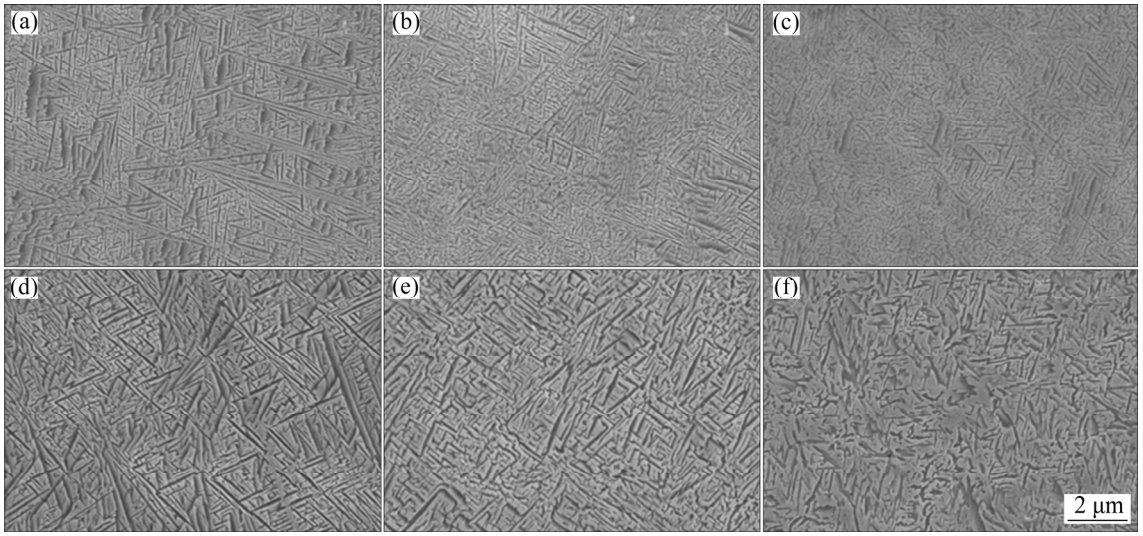

Fig. 6 SEM images of Ti5553−xFe specimens aged at 600 °C for 6 h (a−c) and 24 h (d−f): (a, d) Ti5553; (b, e) Ti5553−1.27Fe; (c, f) Ti5553−2Fe

3.4 Solution strengthening and age hardening behavior

Figure 7(a) shows variations of Vickers hardness as a function of Fe-addition in the solution-treated Ti5553−xFe specimens. It can be seen that the hardness increases with incremental Fe-addition. For the aged specimens, the hardness increment is strongly depended on Fe-additions, as shown in Fig. 7(b). As for sample aged for 5 min, the Vickers hardness in Fe-free Ti5553 specimen rapidly increases from HV 320 to HV 516, whereas the increment of hardness in Ti5553−1.2Fe and Ti5553−2Fe is HV 34 and 26, respectively. After being aged for 30 min, the hardness of Ti5553−2Fe slightly exceeds that of other alloys. This indicates that Fe-addition delays the aging response of Ti5553 alloy. The hardening behavior of Ti5553−xFe specimens during further aging treatment is shown in Fig. 7(c). The curves exhibit an ordinary evolution which is composed of

underaged, peak-aged and overaged stage in sequence with increasing aging time. Additionally, it is noted that Ti5553−2Fe specimen has prominent hardness on both the solid solution condition and peak-aged condition.

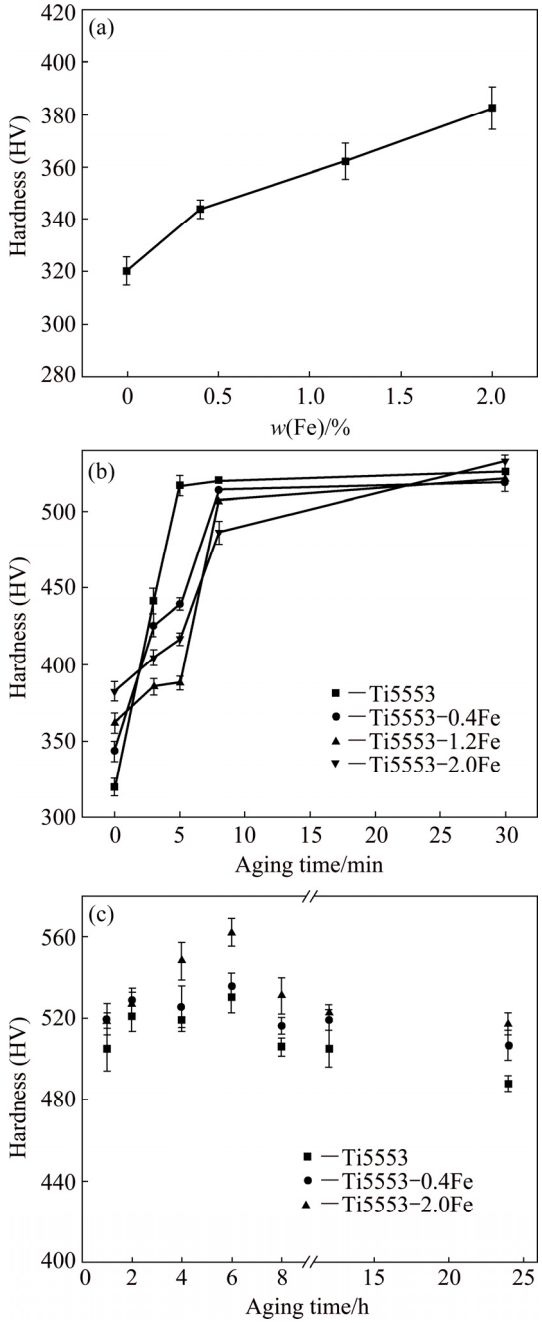

Fig. 7 Variations of Vickers hardness as function of Fe-addition in Ti5553−*x*Fe alloy: (a) Solution-treated specimens; (b) Early stage of aging for specimens aged at 600 °C; (c) Aged specimens at 600 °C for different time

4 Discussion

4.1 Nucleation and growth of α-precipitates

There are three features of α-precipitates in Fe-modified Ti5553 alloys on the basis of experimental results presented above:

(1) The aging response is delayed by Fe-addition, namely a longer incubation time is required for α-precipitation.

(2) The preferential tendency of α_{GB} formation is promoted by Fe-addition, especially in furnace cooling.

(3) A finer dispersion of intergranular α is acquired by increasing Fe-addition. The density of α-lamella with length over 1 μm is conspicuously decreased in Ti5553−2Fe alloy.

In order to make a comprehensive explanation of these features, the classical nucleation and growth theory based on thermodynamics and diffusion is used. Considering the shortage of relevant thermodynamic data in Ti5553 alloy, the prototypical Ti−Mo binary system is used to analyze $\beta\rightarrow\alpha$ transformation instead. The total free energy of α- and β-phase at 600 °C based on Pandat calculation is presented in Fig. 8. The Mo-equivalency value for Ti5553 and Ti5553−2Fe both lies on the right side of the intersection compositional point c_0 on the free energy curves (at 600 °C, c_0 is calculated to be ~8.7 wt.%). Figure 8(b) schematically shows the free energy variation as a function of β-stabilizer content. It is clear that the driving force ΔG of phase transformation decreases with increasing Fe-addition, and the nucleation driving force ΔG_V also reduces obviously. According to the classical nucleation theory, the incubation time τ has

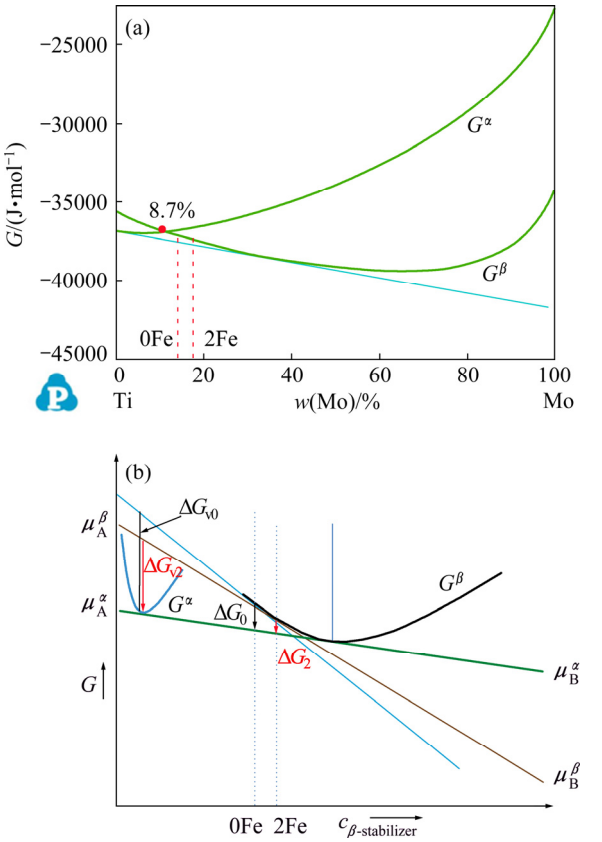

Fig. 8 Gibbs free energy curves for Ti−Mo binary system as function of composition at 600 °C: (a) Pandat calculation results; (b) Schematic illustration relevant to Ti−Mo system differentiating ΔG_V of Fe-modified Ti5553 alloys

a simple relationship with ΔG_V as $\tau \propto \Delta G_V^{-2}$ [29]. Thus, the resultant incubation time is prolonged owing to the inverse proportion between τ and ΔG_V^2.

The driving force of nucleation ΔG_V reduces either at elevated temperature or increased Fe-content. When the specimen is aged at high temperature or furnace cooled from β-phase, the driving force of nucleation is lower especially for the high Fe-content Ti5553 alloy, e.g., Ti5553−2Fe. The β-grain boundary favors the nucleation of α-phase because high-density defects here lower the critical nucleation energy. Hence, preferential tendency of α_{GB} formation with increasing Fe-addition is observed especially during furnace cooling. On the contrary, when being aged at a relatively low temperature, the nucleation driving force becomes much higher. The role of β-grain boundary in decreasing the critical nucleation energy becomes negligible in comparison to ΔG_V, resulting in the suppression of preferential tendency of α_{GB} formation at low-temperature aging treatment [30].

A finer dispersion of intergranular α-precipitates indicates a relatively slow phase growth in Ti5553−1.2Fe and Ti5553−2Fe alloys. During low-temperature aging treatment of β-Ti alloys, Burgers orientation relationship (i.e., $(110)_\beta//(0001)_\alpha$ and $[1\bar{1}1]_\beta//[11\bar{2}0]_\alpha$) is satisfied between α-lamella and β-matrix in order to minimize the lattice misfit. The migration of the broad face closely parallel to $(11\ 11\ \overline{13})_\beta$ plane is strongly limited by the low ledge growth of stable semi-coherent interface [31]. Hence, the width of α-lamella is approximately unchanged regardless of Fe-content after aging treatment. Fe-addition mainly influences the length of α-lamella where long range diffusion is required. Herein, the classical kinetic equation is introduced to explain the different growth behaviors of α-lamella along the long axis direction. Considering the requirement of long range compositional diffusion, the growth velocity v can be written as [30]

$$v = v_0 \exp\left[\frac{Q_G}{RT}\right]\left[1-\exp\left(\frac{\Delta G}{RT}\right)\right] \quad (1)$$

where v_0 is the pre-exponential factor of growth, Q_G is the activation energy of diffusion and ΔG is the chemical free energy difference. It is obvious that a lower $|\Delta G|$ leads to a slower growth rate on basis of Eq. (1). At the beginning of nucleation in Ti5553 and Ti5553−2Fe, owing to the high nucleation driving force ΔG_V discussed above, nucleation in both alloys is believed very quick and a number of α-nucleus form. Subsequently, because of its particularly high diffusion rate of Fe-element [32], Fe atom is quickly rejected into adjacent β-area. The Fe-enrichment stabilizes adjacent β-phase whilst the value of ΔG_V is quickly decreased, which results in a suppression of α-growth in Ti5553−2Fe. During further aging, the growth of initial α-precipitates is accompanied by the formation of new α-nucleus. Consequently, the difference in growth velocity and the continuous α-precipitation can subsequently develop into a higher density of long α lamella in Fe-free Ti5553 specimens (as seen in Fig. 5(a) and Fig. 6(a)) and finer α lamella in Ti5553−2Fe alloy (as clearly seen in Fig. 5(c) and Fig. 6(c)).

4.2 Mechanism of solid solution strengthening and age hardening behavior

Vickers hardness curves in Fig. 7 show that Fe-addition has a strong strengthening effect in both the solid-solution condition and aging condition. The occurrence of solid-solution strengthening originates from two factors: (1) lattice misfit ε_b ($\varepsilon_b=[\delta a(c)/\delta c]/a$) of the solutes positioned in β-matrix, and (2) the modulus misfit ε_G ($\varepsilon_G=[\delta G(c)/\delta c]/G$) caused by solute atoms [33]. Here, a and G are lattice constant and shear modulus in pure metal, respectively, and c is the concentration of solute elements. Then, the combination of these two misfits is expressed as

$$\varepsilon_L = \sqrt{(\varepsilon_G')^2 + (\alpha\varepsilon_b)^2},\ \alpha=9-16,\ \ \varepsilon_G' = \frac{\varepsilon_G}{1+0.5|\varepsilon_G|} \quad (2)$$

Then, the Labusch−Nabarro model in combination with Gypen−Deruyttere approach is utilized [34]. The solid-solution hardening of i element H_i could be expressed as [34,35]

$$H_i = 3G_i\varepsilon_{L_i}^{4/3} \quad (3)$$

In order to obtain the solid-solution hardening of i element H_i, *ab initio* method formulated within the Exact Muffin−Tin Orbitals (EMTO) formalism applying the Coherent Potential Approximation (CPA) is introduced to calculate the lattice constant a_i, shear modulus G_i and ε_{L_i} in binary system. Finally, the solid-solution hardening of multicomponent system is calculated by the Gypen−Deruyttere approach which makes a weighted summation of hardening contribution of each alloying elements [35,36]:

$$H_{SS} = \left(\sum\nolimits_i H_i^{3/2} c_i\right)^{2/3} \quad (4)$$

Figure 9 shows the calculation results relevant to different Fe-additions. Obviously, Ti5553−2Fe alloy possesses ~1.2 times solid-solution hardening in comparison to Fe-Free Ti5553 alloy. This ratio is the same as the ratio of Vickers hardness between Ti5553−2Fe specimen (~HV 390) and Fe-Free Ti5553 specimen (~HV 320) subjected to the solution treatment. In general, the solid solution strengthening is mainly attributed to large lattice misfit ε_b and modulus misfit ε_G induced by Fe-addition.

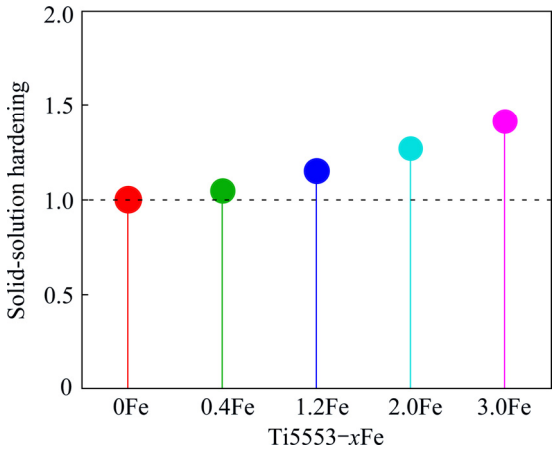

Fig. 9 Solid-solution hardening of Fe-addition in Ti5553 alloys based on *ab initio* method to calculate lattice misfit and shear modulus misfit

With regard to aging treatment, α-phase of submicron in width precipitates from β-matrix, which causes precipitation-hardening [2,37]. At early stage of aging, owing to a low nucleation driving force of Ti5553−2Fe, a sluggish aging response is represented, which results in a lower increment of hardness compared to Fe-free Ti5553 alloy. During further aging, the hardness gradually increases to a peak at 6 h aging and Ti5553−2Fe alloy exhibits the highest hardness (Fig. 7). The difference of the peak hardness is attributed to a finer α phase distribution. As clearly seen in Fig. 5 and Fig. 6, finer α phase distributes in Ti5553−2Fe alloy. Meanwhile, β-matrix is severely divided in discontinuous small regions. This microstructure (i.e., finer α phase and abundant α/β interface) decreases the effective slip length in both thin α lamella and separated β matrix. The decrease in slip length can enhance long-range back stress and effectively hinder dislocation glide [38,39], which in turn effectively strengthen Ti5553−2Fe alloy.

5 Conclusions

(1) The 2 wt.% Fe-addition in Ti5553 alloy suppresses the formation of athermal ω-phase after water quenching from 1000 °C (above the β transus temperature) while the homogeneously distributed ω-precipitates with several nanometers are presented in Fe-free Ti5553 alloy.

(2) Fe-addition increases the stability of β phase and delays α precipitation in Ti5553−xFe alloy. Fe-addition brings about less density of α with length over 1 μm, which is related to the decrease of driving force ΔG_V.

(3) Fe has a strong strengthening effect in both the solution condition and aging condition. The hardness grows incrementally to a peak value for samples with 6 h aging and then declines with increasing aging time to 12 h. Ti5553−2Fe alloy has the highest peak hardness which is on account of both the finely distributed α-precipitates and strong solid-solution strengthening in β-matrix induced by Fe-addition.

Acknowledgments

The authors thank Researcher Sheng-wu GUO for her meaningful help on TEM observation and insightful comments on the manuscript.

References

[1] BANIA P J. Beta titanium alloys and their role in the titanium industry [J]. JOM, 1994, 46: 16−19.
[2] TERLIND G T, DUERIG T W, WILLIAMS J C. Microstructure, tensile deformation, and fracture in aged Ti−10V−2Fe−3Al [J]. Metallurgical Transactions A, 1983, 14: 2101−2115.
[3] FAN J K, LI J S, KOU H C, HUA K, TANG B, ZHANG Y. Microstructure and mechanical property correlation and property optimization of a near β titanium alloy Ti-7333 [J]. Journal of Alloys and Compounds, 2016, 682: 517−524.
[4] BANERJEE D, WILLIAMS J C. Perspectives on titanium science and technology [J]. Acta Materialia, 2013, 61: 844−879.
[5] NYAKANA S L, FANNING J C, BOYER R R. Quick reference guide for β titanium alloys in the 00s [J]. Journal of Materials Engineering and Performance, 2005, 14: 799−811.
[6] XIN X U, DONG L M, ZHANG Z Q, YANG R. Hot deformation behavior and microstructural evolution of beta C titanium alloy in β phase field [J]. Transactions of Nonferrous Metals Society of China, 2016, 26: 2874−2882.
[7] LI Hui-min, LI Miao-quan, LUO J, WANG K. Microstructure and mechanical properties of heat-treated Ti−5Al−2Sn−2Zr− 4Mo−4Cr [J]. Transactions of Nonferrous Metals Society of China, 2015, 25: 2893−2900.
[8] IVASISHIN O M, MARKOVSKY P E, MATVIYCHUK Y V, FOX S. A comparative study of the mechanical properties of high-strength β-titanium alloys [J]. Journal of Alloys and Compounds, 2008, 457: 296−309.
[9] ANKEM S, MARGOLIN H, GREENE C A, OBERSON P G. Mechanical properties of alloys consisting of two ductile phases [J]. Progress in Materials Science, 2006, 51: 632−709.
[10] KANOU O, FUKADA N, HAYAKAWA M. The effect of Fe addition on the mechanical properties of Ti−6Al−4V alloys produced by the prealloyed powder method [J]. Materials Transactions, 2016, 57: 681−685.
[11] DEVARAJ A, JOSHI V V, SRIVASTAVA A, MANANDHAR S, MOXSON V, LAVENDER C. A low-cost hierarchical nanostructured beta-titanium alloy with high strength [J]. Nature Communications, 2016, 7: 11176.
[12] BOLZONI L, RUIZ-NAVAS E M, GORDO E. Understanding the properties of low-cost iron-containing powder metallurgy titanium alloys [J]. Materials and Design, 2016, 110: 317−323.
[13] da COSTA F H, SALVADOR C A F, de MELLO M G, CARAM R. Alpha phase precipitation in Ti−30Nb−1Fe alloys-phase transformations in continuous heating and aging heat treatments [J]. Materials Science and Engineering A, 2016, 677: 222−229.
[14] IBRAHIM K M, MHAEDE M, WAGNER L. Microstructure evolution and mechanical properties of heat treated LCB titanium alloy [J]. Transactions of Nonferrous Metals Society of China, 2012, 22: 2609−2615.
[15] CHEN B Y, HWANG K S. Effect of cooling process on the α phase formation and mechanical properties of sintered Ti−Fe alloys [J].

Materials Science and Engineering A, 2011, 528: 4556−4563.
[16] HSU H C, HSU S K, WU S C, LEE C J, HO W F. Structure and mechanical properties of as-cast Ti−5Nb−*x*Fe alloys [J]. Materials Characterization, 2010, 61: 851−858.
[17] MIN X H, EMURA S, ZHANG L, TSUZAKI K. Effect of Fe and Zr additions on ω phase formation in β-type Ti−Mo alloys [J]. Materials Science and Engineering A, 2008, 497: 74−78.
[18] MIN X H, EMURA S, NISHIMURA T, TSUCHIYA K, TSUZAKI K. Effects of Fe addition on tensile deformation mode and crevice corrosion resistance in Ti−15Mo alloy [J]. Materials Science and Engineering A, 2010, 527: 2693−2701.
[19] MIN X H, TSUZAKI K, EMURA S, TSUCHIYA K. Enhancement of uniform elongation in high strength Ti−Mo based alloys by combination of deformation modes [J]. Materials Science and Engineering A, 2011, 528: 4569−4578.
[20] FANNING J C. Properties of TIMETAL 555 (Ti−5Al−5Mo−5V−3Cr−0.6Fe) [J]. Journal of Materials Engineering and Performance, 2005, 14: 788−791.
[21] ZHENG Y, WILLIAMS R E A, WANG D, SHI R, NAG S, KAMI P, SOSA J M, WANG Y, FRASER H L. Role of ω phase in the formation of extremely refined intragranular α precipitates in metastable β-titanium alloys [J]. Acta Materialia, 2016, 103: 850−858.
[22] JONES N G, DASHWOOD R J, JACKSON M, DYE D. β phase decomposition in Ti−5Al−5Mo−5V−3Cr [J]. Acta Materialia, 2009, 57: 3830−3839.
[23] NAG S, ZHENG Y, WILLIAMS R E A, BOYNE A, FRASER H L. Non-classical homogeneous precipitation mediated by compositional fluctuations in titanium alloys [J]. Acta Materialia, 2012, 60: 6247−6256.
[24] KAR S K, SUMAN S, SHIVAPRASAD S, BHATTACHARJEE A. Processing−microstructure−yield strength correlation in a near β Ti alloy Ti−5Al−5Mo−5V−3Cr [J]. Materials Science and Engineering A, 2014, 610: 171−180.
[25] QIN D, LU Y, LIU Q, ZHOU L. Effects of Si addition on mechanical properties of Ti−5Al−5V−5Mo−3Cr alloy [J]. Materials Science and Engineering A, 2013, 561: 460−467.
[26] OPINI V C, SALVADOR C A F, CHAVES R R, CARAM R. α phase precipitation and mechanical properties of Nb-modified Ti-5553 alloy [J]. Materials Science and Engineering A, 2016, 670: 112−121.
[27] CAMPO K N, ANDRADE D R, CARAM R. On the hardenability of Nb-modified metastable beta Ti-5553 alloy [J]. Journal of Alloys and Compounds, 2016, 667: 211−218.
[28] BALACHANDRAN S, KASHIWAR A, CHOUDHURY A, BANERJEE D, SHI R, WANG Y. On variant distribution and coarsening behavior of the α phase in a metastable β titanium alloy [J]. Acta Materialia, 2016, 106: 374−387.
[29] CAPDEVILA C, ANDRÉS C G, CABALLERO F G. Incubation time of isothermally transformed allotriomorphic ferrite in medium carbon steels [J]. Scripta Materialia, 2001, 44: 129−134.
[30] LIU F, SOMMER F, BOS C, MITTEMEIJER E J. Analysis of solid state phase transformation kinetics: Models and recipes [J]. International Materials Reviews, 2007, 52: 193−212.
[31] YE F, ZHANG W Z, QIU D. A TEM study of the habit plane structure of intragranular proeutectoid α precipitates in a Ti−7.26wt%Cr alloy [J]. Acta Materialia, 2004, 52: 2449−2460.
[32] CARMAN A, ZHANG L C, IVASISHIN O M, PERELOMA E V. Role of alloying elements in microstructure evolution and alloying elements behaviour during sintering of a near-β titanium alloy [J]. Materials Science and Engineering A, 2011, 528: 1686−1693.
[33] ZHANG H, JOHANSSON B, AHUJA R, VITOS L. First-principles study of solid-solution hardening in steel alloys [J]. Computational Materials Science, 2012, 55: 269−272.
[34] LABUSCH R. Statistical theories of solid solution hardening [J]. Acta Metallurgica, 1972, 20: 917−927. (in Germen)
[35] GYPEN L A, DERUYTTERE A. Multi-component solid solution hardening [J]. Journal of Materials Science, 1977, 12: 1034−1038.
[36] TODA-CARABALLO I, RIVERA-DÍAZ-DEL-CASTILLO P E J. Modelling solid solution hardening in high entropy alloys [J]. Acta Materialia, 2015, 85: 14−23.
[37] HE B, LI J, CHENG X, WANG H M. Brittle fracture behavior of a laser additive manufactured near-β titanium alloy after low temperature aging [J]. Materials Science and Engineering A, 2017, 699: 229−238.
[38] WU X, YANG M, YUAN F, WU G, WEI Y, HUANG X, ZHU Y. Heterogeneous lamella structure unites ultrafine-grain strength with coarse-grain ductility [J]. Proceedings of the National Academy of Sciences of the United States of America, 2015, 112: 14501−14505.
[39] MANTRI S A, CHOUDHURI D, ALAM T, VISWANATHAN G B, SOSA J M, FRASER H L, BANERJEE R. Tuning the scale of α precipitates in β-titanium alloys for achieving high strength [J]. Scripta Materialia, 2018, 154: 139−144.

Fe 含量对 Ti5553 合金 α 相析出响应与硬化行为的影响

朱文光[1]，李 沛[1]，孙 逊[2]，陈 威[1]，张华磊[2]，孙巧艳[1]，刘 彬[3]，肖 林[1]，孙 军[1]

1. 西安交通大学 金属材料强度国家重点实验室，西安 710049；
2. 西安交通大学 前沿科学与技术研究院，西安 710049；
3. 中南大学 粉末冶金国家重点实验室，长沙 410083

摘 要：利用混合元素烧结法制备含 0、0.4、1.2 和 2.0 wt.% Fe 的 Ti5553 合金。研究 Fe 元素对绝热 ω 相变、α 相析出长大以及时效硬化行为的影响规律。结果表明，2 wt.% Fe 元素的加入可提高 β 相的稳定性，抑制绝热 ω 相析出。随着 Fe 含量增加，α 相析出孕育期变长，尺寸变小。α 相沿晶析出倾向增强，尤其是在炉冷时，Ti5553−2Fe 合金形成明显的魏氏组织。随后，利用 Pandat 软件并结合经典动力学理论分析 Fe 含量对 Ti5553 合金 α 相析出长大行为的影响机制。硬度曲线表明，不同 Fe 含量合金的硬度均随时效时间延长先增加，6 h 达到峰值后缓慢降低。Ti5553−2Fe 合金具有最高的峰值硬度，这是 Fe 等合金元素点阵错配引起的固溶强化与细小 α 相析出引起的时效强化共同作用的结果。

关键词：Fe 改性 Ti5553 合金；α 相析出长大；硬化行为；Pandat 计算

(Edited by Bing YANG)